Design sensitivity and mixing uniformity of a micro-fluidic mixer

Benjamin Ivorra, Juana López Redondo, Angel M. Ramos, and Juan G. Santiago

Citation: Physics of Fluids **28**, 012005 (2016); doi: 10.1063/1.4939006
View online: http://dx.doi.org/10.1063/1.4939006
View Table of Contents: http://scitation.aip.org/content/aip/journal/pof2/28/1?ver=pdfcov
Published by the AIP Publishing

PHYSICS OF FLUIDS **28**, 012005 (2016)

Design sensitivity and mixing uniformity of a micro-fluidic mixer

Benjamin Ivorra,[1,a)] Juana López Redondo,[2] Angel M. Ramos,[1] and Juan G. Santiago[3]

[1]*Dept. de Matemática Aplicada & Instituto de Matemtica Interdisciplinar, Universidad Complutense de Madrid, Plaza de Ciencias, 3, 28040 Madrid, Spain*
[2]*Dept. de Informática & Campus de Excelencia Internacional Agroalimentario (ceiA3), Universidad de Almería. Ctra. Sacramento, s/n, 04120 La Cañada de San Urbano, Almería, Spain*
[3]*Mechanical Engineering Department, Stanford University, 440 Escondido Mall, Stanford, California 94305-3030, USA*

(Received 28 January 2015; accepted 14 December 2015; published online 15 January 2016)

We consider a particular hydrodynamic focusing microfluidic mixer used to initiate the folding process of individual proteins, which has been designed in a previous work and exhibited a mixing time of 0.1 μs. The aim of the current paper is twofold. First, we explore the sensitivity of mixing time to key geometric and flow parameters. In particular, we study the angle between inlets, the shape of the channel intersections, channel widths, mixer depth, mixer symmetry, inlet velocities, working fluid physical properties, and denaturant concentration thresholds. Second, we analyze the uniformity of mixing times as a function of inlet flow streamlines. We find the shape of the intersection, channel width, inlet velocity ratio, and asymmetries have strong effects on mixing time; while inlet angles, mixer depth, fluid properties, and concentration thresholds have weaker effects. Also, the uniformity of the mixing time is preserved for most of the inlet flow and distances of down to within about 0.4 μm of the mixer wall. We offer these analyses of sensitivities to imperfections in mixer geometry and flow conditions as a guide to experimental efforts which aim to fabricate and use these types of mixers. Our study also highlights key issues and provides a guide to the optimization and practical design of other microfluidic devices dependent on both geometry and flow conditions. © *2016 AIP Publishing LLC.* [http://dx.doi.org/10.1063/1.4939006]

I. INTRODUCTION

Protein folding studies[1,2] pose a great challenge to microfluidic mixers. In this work, we consider a class of microfluidic mixers based on diffusion from (or to) a hydrodynamically focused stream, of a type initially proposed by Brody *et al.*[3] The basic features of the design are as follows: It is composed of three inlet channels and a common outlet channel, and the geometry has a symmetry with the center channel. A geometrical representation of such a mixer is shown in Figure 1 (here, the mixer proposed in Ref. 4). Typically, a mixture of unfolded proteins and a chemical denaturant solution is injected through the center channel and exposed to background buffers (no denaturant) streams through the two side channels. The design goal is to rapidly decrease the denaturant concentration in order to rapidly initiate protein folding in the outlet channel.[1] Since the publication of Brody *et al.*, there have been significant advances on the design of these mixers,[5–8] in particular, regarding the reduction of the mixing time (i.e., the time required to reach a sufficiently low denaturant concentration).

We recently studied (see Ref. 4) the optimization of the shape and flow conditions of a particular hydrodynamic focused microfluidic mixer. The objective was to improve the mixing time of the best mixer designs found in the literature, which exhibited mixing times of approximately 1.0 μs.[7] The

a)Author to whom correspondence should be addressed. Electronic mail: ivorra@mat.ucm.es

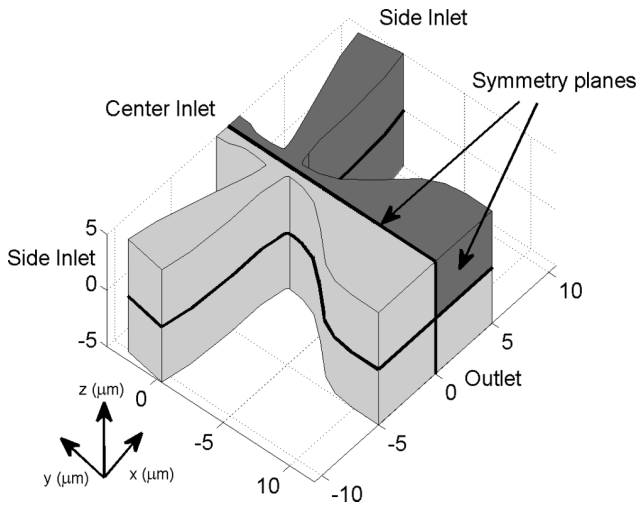

FIG. 1. Typical three-dimensional representation of the microfluidic mixer geometry. The mixer design hydrodynamically focuses a center inlet stream using two side inlets. In dark gray, we represent the domain Ω used for numerical simulations. The geometry's two symmetry planes are also highlighted.

optimized mixer generated by our approach achieved a mixing time of about 0.10 μs. The shape of this optimized microfluidic mixer and its concentration distribution is summarized in Figure 2. The optimization problem studied in this previous work was identified as highly nonlinear.[9–11] Further, the process has many parameters which are difficult to know with great precision in experiments.

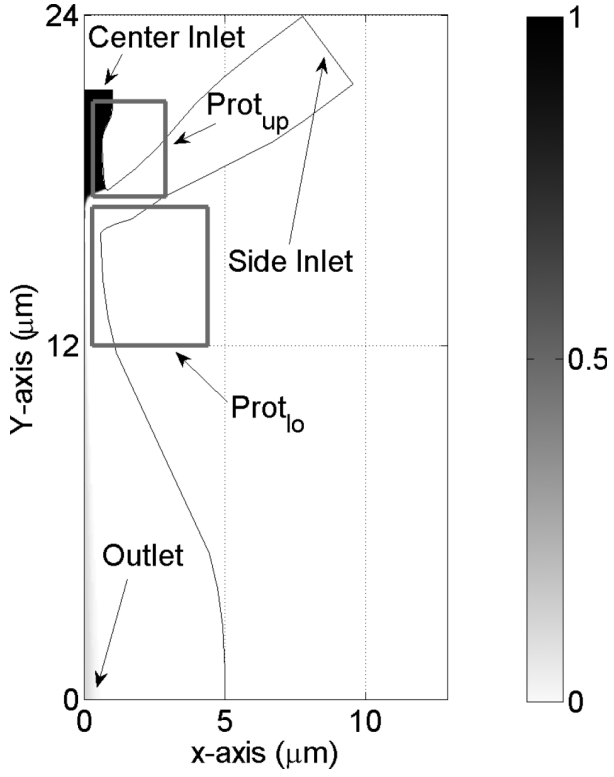

FIG. 2. Optimized mixer of Ref. 4: Top view representation of the half of the mixer shape (symmetry with respect to $x = 0$ μm) with a superposed grey scale plot of the denaturant normalized concentration distribution c at width $z = 0$ μm. The parts of the mixer shape corresponding to the protuberances Prot_{up} and Prot_{lo}, as introduced in Section IV A 2, are also highlighted.

Therefore, it is important to understand and quantify the stability of the device performance with respect to these parameters. This enables identification of key parameters and so guide experimental efforts. To this aim, we presented a very simple sensitivity analysis in Ref. 4 that consisted of normalized random perturbations of all the parameters and showed that the mixing time variations were of the same order as the perturbations considered, suggesting the optimized solution was fairly stable.

Here, we significantly increase the scope of our sensitivity analysis. We quantify the impact of mixing time on the key design parameters of the mixer. The objective of our study is to provide recommendations and guidelines for the fabrication of the device introduced here. More precisely, we consider and study (i) geometrical parameters defining the mixer shape: the angle defined by the channel intersection, the shape of the channel intersection, the width of the inlet and outlet channels, the mixer depth and possible irregularities in the symmetry of the shape; (ii) central and side injections velocities; and (iii) physical coefficients associated with the working fluid and the concentration thresholds of the mixing time definition.

In addition to those sensitivity analysis experiments, we also analyze the uniformity of the mixing time as a function of the inlet streamline location in the inlet channel. This mixing time uniformity analysis quantifies the robustness of the mixing time through the whole inlet flow and helps placing a statistical confidence on observed mixing times. In particular, it helps quantifying the so-called wall effect (due to the no-slip condition at the mixer walls, resulting in low velocity values near the walls) on mixer performance.

The last two decades have seen a large number of microfluidic device designs and their use in a wide range of applications. Most, if not all, of these devices have performance specifications which are dependent on their geometry and flow control conditions (e.g., flow rates, pressure, and inlet concentrations). Despite this, the systematic study of how performance depends on intentional or unintentional design parameters is rarely if ever demonstrated. For this reason, we also offer the current work as a case study describing the significant challenge and complexity of determining design robustness for microfluidics.

This article is organized as follows: Section II introduces the 3D model used to estimate the mixing times. Section III describes the mixing time uniformity analysis and the results. Section IV presents the numerical experiments carried out to perform the extended sensitivity analysis and deduce major conclusions and design guidelines.

II. MICROFLUIDIC MIXER MODELING

We consider the microfluidic mixer described in Section I. The geometry has two symmetry planes which we use to reduce the simulation domain to a quarter of the mixer. This reduced domain is denoted by Ω, as depicted in Figure 1. The mixer shape is composed of interpolated surfaces, and the inlet velocities are described by a set of parameters denoted by ϕ, detailed in Ref. 4. We consider guanidine hydrochloride (GdCl)[1,12] as the denaturant.

We assume the flow velocity and the denaturant concentration distribution can be approximated by using the steady configurations of the incompressible Navier-Stokes equations coupled with the convective diffusion equation[5,6] as follows:

$$\begin{cases} -\nabla \cdot (\eta(\nabla \mathbf{u} + (\nabla \mathbf{u})^{\top}) - p\mathbf{I}) + \rho(\mathbf{u} \cdot \nabla)\mathbf{u} = 0 & \text{in } \Omega, \\ \nabla \cdot \mathbf{u} = 0 & \text{in } \Omega, \\ \nabla \cdot (-D\nabla c) + \mathbf{u} \cdot \nabla c = 0 & \text{in } \Omega, \end{cases} \tag{1}$$

where c is the denaturant normalized concentration distribution, $\mathbf{u}$ is the flow velocity vector (m s^{-1}), p is the pressure field (Pa), $D = 2 \times 10^{-9}$ is the diffusion coefficient of the denaturant solution in the background buffer (m^2 s^{-1}), $\eta = 9.8 \times 10^{-4}$ is the denaturant solution dynamic viscosity (kg m^{-1} s^{-1}) and $\rho = 1010$ is the denaturant solution density (kg m^{-3}).

System (1) is completed with the following boundary conditions:

$$\begin{cases} \mathbf{u} = 0 & \text{on } \Gamma_w, \\ \mathbf{u} = -u_s \text{para}_1 \mathbf{n} \quad \text{and} \quad c = 0 & \text{on } \Gamma_s, \\ \mathbf{u} = -u_c \text{para}_2 \mathbf{n} \quad \text{and} \quad \mathbf{n} \cdot (-D\nabla c + c\mathbf{u}) = -c_0 \mathbf{u} & \text{on } \Gamma_c, \\ p = 0 \text{ and } (\eta(\nabla \mathbf{u} + (\nabla \mathbf{u})^\top))\mathbf{n} = 0 \quad \text{and} \quad \mathbf{n} \cdot (-D\nabla c) = 0 & \text{on } \Gamma_e, \\ \mathbf{n} \cdot \mathbf{u} = 0 \text{ and } \mathbf{t} \cdot (\eta(\nabla \mathbf{u} + (\nabla \mathbf{u})^\top) - p\mathbf{I})\mathbf{n} = 0 & \text{on } \Gamma_a, \\ \mathbf{n} \cdot (-D\nabla c + c\mathbf{u}) = 0 & \text{on } \Gamma_w \cup \Gamma_a, \end{cases} \tag{2}$$

where Γ_c, Γ_s, Γ_e, Γ_w, and Γ_a denote the boundaries representing the central inlet, the side inlet, the outlet, the mixer walls, and the symmetry plane, respectively; u_s and u_c are the maximum side and center channel injection velocities (m s^{-1}), respectively; para_1 and para_2 are the laminar flow profiles, which are equal to 0 in the inlet border and to 1 in the inlet center, of the side and central inlets, respectively;[13] $c_0 = 1$ is the initial denaturant normalized concentration in the center inlet; and $(\mathbf{t}, \mathbf{n})$ is the local orthonormal reference frame along the boundary.

In this work, the mixing time of a particular mixer ϕ, denoted by $J(\phi)$ is defined as the time required to change the denaturant normalized concentration of a typical Lagrangian stream fluid particle situated in the symmetry streamline at depth $z = 0$ μm from α% to ω%. It is computed by

$$J(\phi) = \int_{c_\omega^\phi}^{c_\alpha^\phi} \frac{\mathrm{d}y}{\mathbf{u}^\phi(y)}, \tag{3}$$

where $\mathbf{u}^\phi$ and c^ϕ denote the solution of system (1) and (2), when considering the mixer defined by ϕ; and c_α^ϕ and c_ω^ϕ denote the y-coordinate of points situated along the streamline defined by the intersection of the two symmetry planes $z = 0$ μm and $x = 0$ μm, i.e., the y-axis, where the denaturant normalized concentration c^ϕ is α and ω, respectively. By default, we assume $\alpha = 90\%$ and $\omega = 30\%$.

The numerical model used to approximate the solutions of systems (1) and (2) and to compute (3) was implemented by coupling Matlab scripts with COMSOL Multiphysics 3.5a models. A complete description of this numerical implementation can be found in Ref. 4.

III. UNIFORMITY OF THE MIXING TIME

We first analyze the non-uniformity of mixing times across the focused stream for our optimized mixer ϕ_o. Indeed, as suggested in Refs. 7 and 14, the mixing time can be measured not only in the symmetry streamline, situated on the (x,z) = (0,0) segment, but also in other streamlines. We are interested in the uniformity of mixing times, as protein states in these mixers are quantified experimentally within a finite probe volume which integrates signal throughout a volume in space within the mixing region. This measurement volume is fed, in principle, by all streamlines of the center inlet channel.

We consider 100 streamlines, denoted by $(sl_{i,j})_{i,j=1}^{10}$, starting from a finite set of points, which are denoted by Σ_{Γ_c}, in Γ_c. Here, $\Sigma_{\Gamma_c} = \{P_{(i,j)} | i = 1, \ldots, 10 \text{ and } j = 1, \ldots, 10\}$ where $P_{(i,j)} = (\frac{i}{10}0.9\ \mu\text{m}, \frac{j}{8}0.75\ \mu\text{m})$. In the previous definition, the maximum coordinate in the x-axis (i.e., 0.9 μm) has been selected in order to avoid particles too close to the wall Γ_w, and the maximum coordinate in the z-axis (i.e., 0.75 μm) has been chosen as a characteristic 1.5 μm depth of field for confocal microscope imaging (i.e., extent of the measurement volume).[5] Those streamlines are numerically approximated by considering an explicit Euler scheme and the velocity vector $\mathbf{u}$ obtained by solving system (1) and (2).[2]

For each streamline $sl_{i,j}$, we compute the associated mixing times, denoted by $t_{sl_{i,j}}$, in a manner similar to Equation (3). More precisely, $t_{sl_{i,j}}$ is defined as the time required by a protein within a Lagrangian fluid particle to travel from $c_{90}^{sl_{i,j}}$ to $c_{30}^{sl_{i,j}}$, where $c_{90}^{sl_{i,j}}$ and $c_{30}^{sl_{i,j}}$ denote the points within $sl_{i,j}$ with a concentration of 90% and 30%, respectively. Next, we study the spatial distribution according to the streamline starting point in Σ_{Γ_c}, the maximum value, the mean value, and the standard deviation of $(t_{sl_{i,j}})_{i,j=1}^{10}$. Furthermore, we also compute the weighted mixing time value of $sl_{i,j}$, denoted by $\overline{t_{sl_{i,j}}}$ and defined as

$$\overline{t_{sl_{i,j}}} = \frac{\omega_{i,j} t_{sl_{i,j}}}{\sum_{i,j=1}^{10} \omega_{i,j}}, \tag{4}$$

where $\omega_{i,j}$ denotes the velocity of a particle in the streamline $sl_{i,j}$ at its initial position $x^{\text{init}}_{(i,j)}$. This choice of weight coefficients reflects the fact that the probe volume used to measure experimentally the mixing time receive particles more frequently from streamlines with the highest velocities. The maximum and standard deviation values of those weighted mixing times $(\overline{t_{sl_{i,j}}})_{i,j=1}^{10}$ are also studied.

Furthermore, due to the fact that the depth of the mixer is 10 times larger than the minimum width of the center channel, the mixing time variations in the z-axis direction are negligible in comparison to the variations in the x-axis.[5] Thus, we perform a more extensive uniformity analysis along the x-axis, by considering 100 streamlines, denoted by $(sl_{i,z=0})_{i=1}^{100}$, in the plane $z = 0$ starting from the set of points $P_i = (\frac{i}{100}0.9\ \mu\text{m}, 0\ \mu\text{m})$ in Γ_c. The methodology is the same as that introduced previously. In this case, we also compute the evolution of both the mean value and standard deviation of $(t_{sl_{i,z=0}})_{i=1}^{k}$ and $(\overline{t_{sl_{i,z=0}}})_{i=1}^{k}$, with $k = 1, \ldots, 100$. These results will be compared with the ones presented in Ref. 5. We note that a similar analysis was also performed by considering variations of the protein streamlines along the z-axis. This included streamlines starting from the set $P_i = (0\ \mu\text{m}, \frac{i}{100}0.75\ \mu\text{m})$ in Γ_c. However, in that case, negligible variations of the mixing time (i.e., lower than 0.01 μs) have been observed and those results are not detailed here.

Our study of mixing time uniformity yielded that the mean mixing time value obtained by considering $(t_{sl_{i,j}})_{i,j=1}^{10}$ was 0.34 μs with a standard deviation of 0.17 μs. As expected, the maximum mixing time value was reached at the streamline $sl_{10,10}$ with a value of 1.43 μs.

The mixing times $t_{sl_{i,j}}$ and weighted mixing times $\overline{t_{sl_{i,j}}}$ of the considered streamlines $(sl_{i,j})_{i,j=1}^{10}$ are presented in Figure 3(a). As shown, within 0.4 μm of the centerline, the mixing times vary between 0.1 μs and 0.5 μs, and this region accounts for 60% of the detection events (i.e., considering the sum of the weight coefficients $(\sum_{i=1}^{4}\sum_{j=1}^{10}\omega_{i,j})/(\sum_{i,j=1}^{10}\omega_{i,j})$). In contrast, the near-wall region of [0.7, 0.9] μm of the centerline has mixing times between 1 and 1.43 μs, but these streamlines contribute to only 10% of detection events (i.e., considering $(\sum_{i=7}^{10}\sum_{j=1}^{10}\omega_{i,j})/(\sum_{i,j=1}^{10}\omega_{i,j})$).

Next, the mixing times $t_{sl_{i,z=0}}$ and weighted mixing times $\overline{t_{sl_{i,z=0}}}$ across the streamlines $(sl_{i,z=0})_{i=1}^{100}$ are plotted versus spanwise streamline position in Figure 3(b). For these 100 streamlines, the mean mixing time computed by considering $(t_{sl_{i,z=0}})_{i=1}^{100}$ was 0.32 μs with a standard deviation of 0.16 μs. Again, we can observe that particles near the walls exhibit higher mixing times (>1 μs). However, these near-wall-slow-moving particles contribute only infrequently to probe volume detection events.

We note similar phenomena were reported in Ref. 5. However, the mixer presented in that work exhibited a mean mixing time, considering streamlines in the plane z = 0, of 3.1 μs with a standard deviation of 1.5 μs. The maximum mixing time value was 10 μs, obtained for the streamline closer to the wall Γ_w. The optimized mixer design presented here therefore offers better mixing time uniformity leading to more consistent measurements and less scatter in measurement ensembles.

IV. SENSITIVITY ANALYSIS OF THE MODEL PARAMETERS

We here present a study of the influence of key parameters of the model described in Section II on mixer mixing time. We vary parameters individually, fixing the values of others to the corresponding value of the optimized mixer ϕ_o. We note that, in our previous work, we explored the impact of simultaneous perturbations on the whole set of parameters on mixer performance.[4] We here perform the more complete influence of individual perturbations on the mixing time. We believe such individual parameter perturbation analyses are also more useful to designers in identifying key parameters and methods for fabrication. We consider the following percent variation function:

$$E(\phi_p) = 100\frac{|J(\phi_o) - J(\phi_p)|}{J(\phi_o)}, \tag{5}$$

where ϕ_p represents the perturbed mixer.

The parameters analyzed can be classified in three categories: (i) geometrical parameters defining the mixer shape; (ii) central and side injections velocities; and (iii) physical coefficients associated with the denaturant solution and the concentration threshold in the mixing time definition.

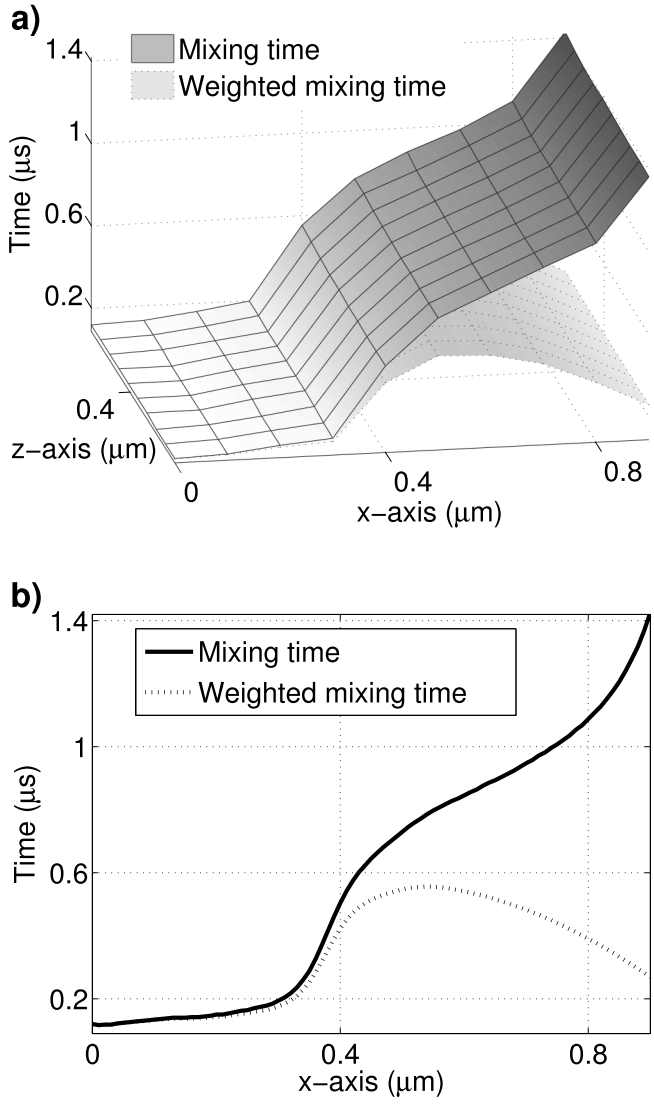

FIG. 3. Results obtained during the analysis of the mixing time non-uniformity for the optimized mixer: (a) Mixing and weighted mixing times obtained according to the position (x, z) in Γ_c of the initial particle for the considered streamlines, (b) mixing and weighted mixing times obtained as a function of the position x in Γ_c of the initial particle and for the streamlines considered in the plane $z = 0$. The weighted mixing time reflects the frequency of events (measurements of proteins along said streamline) as determined by the stream-line averaged velocity. The lower velocities near the wall yield longer mixing times but are less frequent.

A. Geometrical parameters

In the following computational experiments, we analyze the variation on the mixing time due to changes in: (i) the angle defined at the channel intersection; (ii) the shape of the channel intersection; (iii) the width of the inlet and outlet channels; (iv) the mixer depth; and (v) perturbation in the symmetry of the mixer shape.

1. Inlet intersection angle

First, we study the angle between the x-axis and the mixer side channel, denoted by θ. The optimized value $\theta = \pi/5$ is varied from 0 up to $2\pi/5$ by considering 50 equally spaced intermediate values (i.e, we perform 50 evaluations of our model). A geometrical representation of those variations is showed in Figure 4.

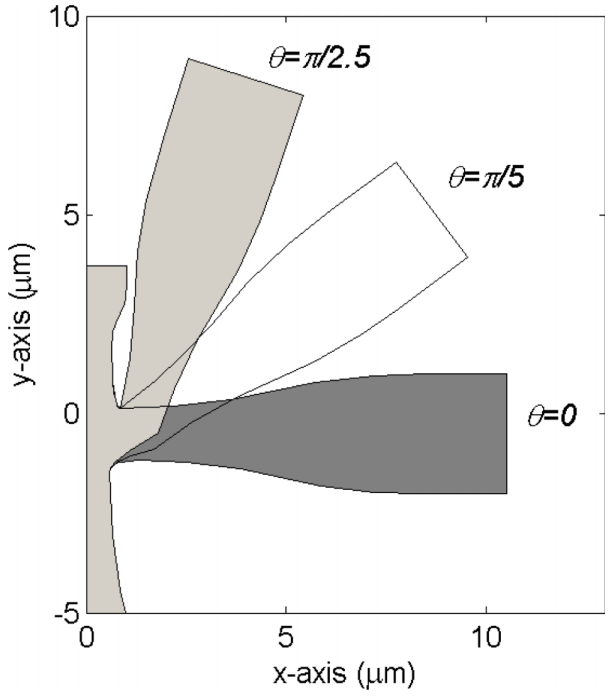

FIG. 4. Three mixer shapes for inlets intersection angles of $\theta = 0$ (light grey), $\theta = \pi/5$ (white), and $\theta = 2\pi/5$ (dark grey). Only the area where the shape changes are shown.

Perturbations on θ have generated a mean variation in the mixing time of 3%. Figure 5 gives a graphical representation of the obtained results. As we can observe on this plot, the maximum variation was around 15% and was obtained for $\theta = 2\pi/5$. Furthermore, the variation was less than 4% for angles lower than $\pi/3$, and grew up exponentially after that value. This suggests that the angle is not a sensible parameter for the mixer performance.

2. Shape of the channel intersection

We now study the impact of the shape of the area where the three inlets and the outlet intersect. The shapes allowed by our model are built by considering Beziers curves and describe a "bubble" (also

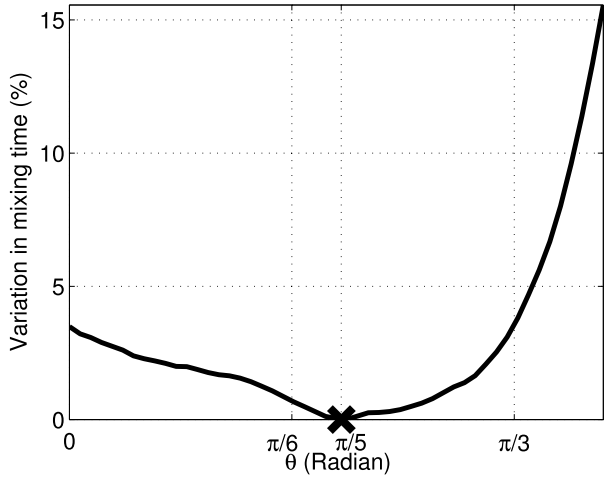

FIG. 5. Percent variation of mixing time as a function of deviation from the optimal angle θ value (denoted by $X = \pi/5$, c.f. Figure 4). Mixing time is relatively insensitive to small errors in angle of the side channel. The distribution shows the strongly non-linear dependence of mixing time on geometry.

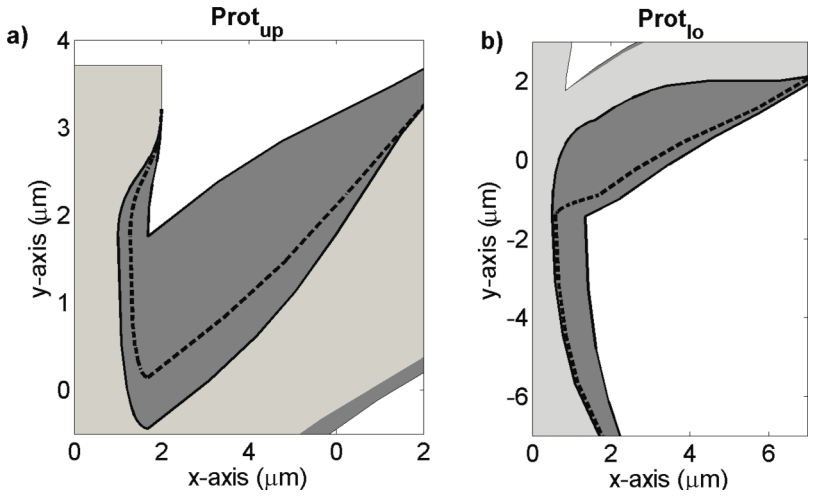

FIG. 6. Mixer shapes highlighting the range of mixer shapes we explored. In both cases, the optimal shape is shown as a dark line. Shown are detailed views of the shape of the channels intersection near the (a) upper (denoted by Prot_{up}) and (b) lower (denoted by Prot_{lo}) corners of the intersection region. The dark gray zones correspond to the domain, between the shape of the maximum and the minimum protuberance allowed by the model considered here (according to a minimum channel width of 1 μm).

called protuberance) invading the central and side inlets from the upper corner (according to y-axis) and a protuberance invading the outlet and side inlets from the lower corner. These protuberances are defined according to a restriction (due to a convenient lithographic and plasma etching limitation) of a minimum channel width of 1 μm. For the sake of simplicity, those bubbles are only described by two scalar numbers Prot_{up} and Prot_{lo} in $[0,1]$, where 0 corresponds to the minimum bubble shape and unity is the maximum bubble shape of the upper and lower corners, respectively, as allowed by the model. The optimal shape corresponds to $\text{Prot}_{\text{up}} = 0.8$ and $\text{Prot}_{\text{lo}} = 0.7$. The parts of the mixer shape corresponding to Prot_{up} and Prot_{lo} are presented in Figure 2. A geometrical representation of the minimum, maximum, and optimal shapes of the protuberances is given in Figure 6.

This experiment consisted of computing the mixing time of the mixer generated by considering all the possible combination of values of Prot_{up} and Prot_{lo} in $[0,1]$ with a grid step size of 0.1. This required 121 evaluations of our model. The variation of the mixing time according to analyzed values of Prot_{up} and Prot_{lo} is presented in Figure 7 and values are reported in Table I. As shown by both

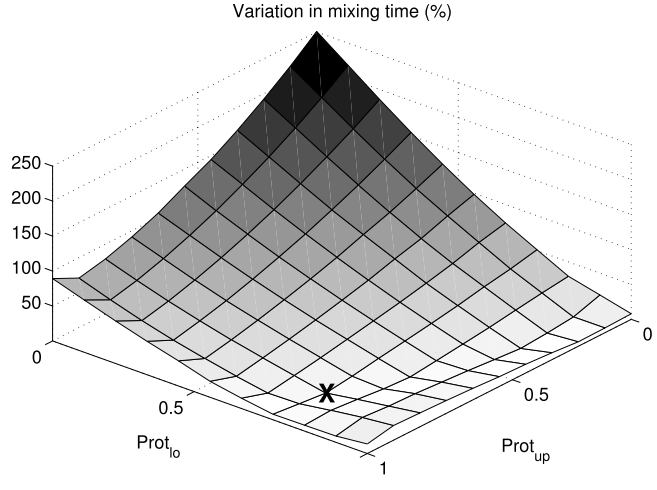

FIG. 7. Percent variation of mixing time for the optimal shape (represented by X) for the protuberance magnitudes considered and described in Section IV A 2. Protuberance parameter values Prot_{up} and Prot_{lo} each varies from 0 to unity with a grid step size of 0.1. The details of the protuberance shape of the side channels are an important feature.

TABLE I. Percentage variation in mixing time of the optimal design value and considering the protuberances described in Section IV A 2. Here protuberances parameters Prot_{up} and Prot_{lo}, each varies from 0 to unity with a grid step size of 0.1. The optimal shape (...) is obtained with $\text{Prot}_{\text{up}} = 0.8$ and $\text{Prot}_{\text{lo}} = 0.7$.

	Prot_{up}										
Prot_{lo}	0.0	0.1	0.2	0.3	0.4	0.5	0.6	0.7	0.8	0.9	1.0
0.0	251	220	192	167	144	126	106	91	79	71	89
0.1	218	192	167	145	125	107	90	76	65	56	75
0.2	186	163	142	123	105	89	75	62	51	42	61
0.3	155	136	118	102	86	73	60	48	39	30	48
0.4	125	110	95	82	69	57	47	37	28	20	36
0.5	98	87	74	64	52	43	34	26	18	11	20
0.6	74	65	54	45	37	29	22	15	9	3	15
0.7	51	43	37	29	23	17	11	5	...	4	8
0.8	30	25	19	14	9	5	1	3	7	11	9
0.9	19	7	3	2	3	7	9	12	14	17	9
1.0	8	7	6	10	13	14	16	19	20	21	14

the figure and the table, for values of Prot_{up} and Prot_{lo} lower than 0.5, the mixing time dramatically increased from 50% up to 250%. This indicates that a minimum protuberance in both upper and lower corners should be considered in order to obtain an efficient mixing time. Furthermore, when Prot_{up} and Prot_{lo} were greater than 0.5, the variation in mixing time was moderated and was lowered by 22%, which can be considered as a reasonable value. In addition to those first results, we see that the impact on the mixing of Prot_{up} was greater than Prot_{lo}. For instance, by decreasing the parameter Prot_{lo} from 1 to 0 and fixing the value of $\text{Prot}_{\text{up}} = 1$, we have generated mixing time variations up to 50%, whereas by decreasing the parameter Prot_{up} and fixing $\text{Prot}_{\text{lo}} = 1$, we have obtained a maximum 20% variation of mixing time. This result is consistent with the fact that the length of the lower corner is much larger than that of the upper (see Figure 6); thus, its influence on the mixing time is expected to be greater.

From the previous results, we conclude that the mixing time is sensitive to the shape of these protuberances.

3. Channel width

We are here interested in estimating the impact of the inlets and outlet widths on the mixing time (i.e., the minimum width of these channels where the flow they carry first interact with the neighbouring streams). This study is interesting as the mixer design and general shape can be scaled geometrically and inserted into different devices. We note that the channel widths were fixed during the optimization process in Ref. 4 and were set to values suited for the mixer implementation and validation studies, as the one carried out in Ref. 5.

We considered a width denoted by $w_c \in [1\ \mu\text{m}, 4\ \mu\text{m}]$ for the central inlet, a width denoted by $w_s \in [1\ \mu\text{m}, 4\ \mu\text{m}]$ for the side inlets and a width denoted by $w_o \in [2\ \mu\text{m}, 18\ \mu\text{m}]$ for the outlet. The original optimized shape exhibited $w_c = 2\ \mu\text{m}$, $w_s = 3\ \mu\text{m}$, and $w_o = 10\ \mu\text{m}$. All possible configurations of channel widths were tested by considering a mesh of step size of $1\ \mu\text{m}$ for each width, which represents a total of 272 evaluations of our model. Representations of the mixer shape with all channel widths set to their maximum or minimum values are depicted by Figure 8.

In order to check the importance of each channel width on the mixing time regarding all possible configurations of other width, we considered percent variations denoted by *WE* and the mean evolution of the mixing time *MET* according to each width. Both processes are explained below. We illustrate the process of computing *WE* and *MET* in the case of w_c. This approach can be extended to w_s and w_o.

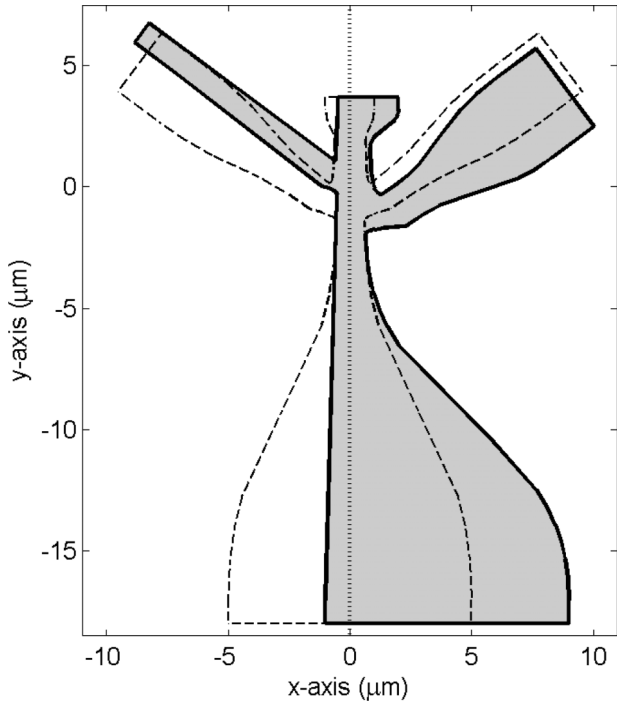

FIG. 8. Shape of the mixer for lengths of the channels set to their maximum (continuous line for $x > 0$ m) values and minimum values (continuous line for $x < 0$ m). The dashed-dotted line corresponds to the axis $x = 0$ (and the y-z symmetry plane). The optimal mixer shape is represented by a dashed line. We note the choice of parameterization of the mixer shape (including side inlet channel width) determines the position of the region corresponding to the channel intersection. Our geometry variations therefore considered a wide range of shapes and relative channel lengths.

The value $WE_{w_c}(j,k)$ represents a measure of the variation of the mixer mixing time according to changes in w_c when other widths are fixed to $w_s = j$ and $w_o = k$ and is given by

$$WE_{w_c}(j,k) = 100\frac{1}{4}\sum_{i=1}^{4}\frac{|J(\phi_{i,j,k}) - \text{mean}_i J(\phi_{i,j,k})|}{\text{mean}_i J(\phi_{i,j,k})}, \tag{6}$$

where $\phi_{i,j,k}$ denotes the mixer obtained by considering $w_c = i, w_s = j, w_o = k$ and the other parameters set to the optimal values and $\text{mean}_i J(\phi_{i,j,k})$ denotes the mean value of the mixing time obtained by varying only i. We compute $WE_{w_c}(j,k)$ for $j = 1,\ldots,4$, $k = 2,\ldots,18$ and report its mean, minimum, and maximum values according to j and k. Those results are reported in Table II.

The value $MTE_{w_c}(i)$ corresponds to the mean values of the mixing times $J(\phi_{i,j,k})$ obtained when considering $j = 1,\ldots,4$ and $k = 2,\ldots,18$. The evolution of MTE_{w_c}, MTE_{w_c}, and MTE_{w_c} is depicted in Figure 9.

TABLE II. Maximum, minimum, and mean values of the mixing time percent variation named *WE*, defined in Section IV A 3, for the widths w_c, w_s, and w_o.

	WE		
Width	Mean	Min	Max
w_c	60	27	103
w_s	68	96	118
w_o	7	1	57

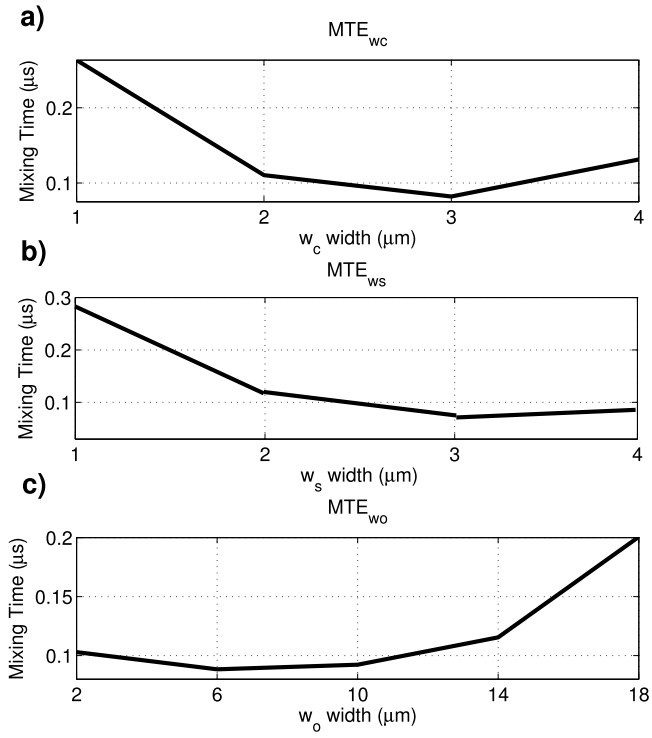

FIG. 9. Dependence of mean values of mixing times as defined in Section IV A 3 as a function of inlet and outlet channel widths. Shown are plots (a) MTE_{w_c}, (b) MTE_{w_s}, and (c) MTE_{w_o} which correspond to the mean mixing times obtained when fixing the value of w_c, w_s, and w_o, respectively, and let the other widths vary. Width variations have a moderate effect on mixing times.

As we can observe in Table II, the most sensitive widths are the side inlets and central inlet with a mean mixing time variation of about 65%. This result is expected, since those inlets carry the denaturant solution and buffer flows, and thus affect the amount of injected products. Significant changes to these inlet geometries should be accompanied by changes in inlet velocities and performing a new optimization process as in Ref. 4. For example, we hypothesize that variations which aim to preserve flow rate ratios should be explored first. On the other hand, outlet widths in the interval [2,13] μm (from the optimal value of 6 μm) will affect mixing time variation by only 7%. Hence, we conclude that such errors on width have only a slight to moderate effect on mixing times. Furthermore, regarding Figure 9, we see that the mean mixing time is lower when considering values of w_c and w_s in the interval [2 μm, 4 μm], and $w_o \in$ [1 μm, 12 μm]. Moreover, we remark that configurations with smaller inlets and bigger outlet are the worst from an efficiency point of view.

4. Mixer depth

Next, we analyzed the effects of the mixer depth (in Z-direction). Imperfections in microfabrication of these mixers can result in depth variations of approximately ± 1 μm.[6] We thus computed the mixing time for mixers generated by considering the set of parameter ϕ_o and depths of 8, 9, 11, and 12 μm. The resulting mixing times (and their associated percent variation regarding the mixing time of the original mixer with a depth of 10 μm) were 0.14 μs (34%), 0.12 μs (13%), 0.10 μs (6%), and 0.09 μs (13%), respectively.

As shown by these results, perturbations of ± 1 μm generate reasonable percent variations in the weighted mean mixing time between 6% and 13%. As described previously, this indicates that errors in the mixer depth due to manufacturing processes do not strongly affect mixing performance for these relatively deep ($\sim$10 μm) mixers. Note that the highest channel depth yields the lowest mixing time (0.09 μs for a depth equal to 12 μm versus 0.14 μs for the 8 μm depth). This result is expected, as

the so-called wall effect (i.e., where the no-slip condition at the top wall results in low velocity values near the wall and near the corner where the X-Y plane meets the Y-Z plane) reduces the mixing performance near the mixer walls. Again, we see that the optimal mixer design (minimum mixing time) is influenced strongly by changes in manufacturing process (namely, in achieving high aspect ratio features with deep reactive ion etching). Mixer designs with relatively high channel-depth-to-feature width ratios yield optimal results. In our study, the minimum channel width (near $y = -1.5$ μm) was 1.1 μm.

5. Shape symmetry

The last geometrical aspect analyzed during this work is the impact of perturbations in the symmetry of the mixer according to the plane $x = 0$ (including nonsymmetric injections velocities) on the mixer characteristics.

To this end, we considered the right half (versus quarter) of the geometry. We then randomly generated 100 nonsymmetric mixers by considering perturbations of the parameters from 0.5% up to 50% of the left side (respecting to $x = 0$) of the mixer shape and by keeping the right side of the mixer shape to its optimal value. These mixers were then classified according to the deviation observed between the streamlines starting from $(x = 0, y = 0, z = 0)$ μm of the symmetric and nonsymmetric mixers at the time when the non-perturbed symmetric streamline reach Γ_e. According to this classification, we then computed the mean mixing time for each category and compared it to the optimized mixer mixing time by considering the percent variation formula (5). Deviations in the intervals [0,0.3] μm, [0.3,0.6] μm, [0.6,0.9] μm, [0.9,1.2] μm, [1.2,1.5] μm, and greater than 1.5 μm generated mean mixing time percent variation of 14%, 64%, 114%, 237%, 328%, and 542%, respectively.

As we can observe from those data, for deviations below 0.3 μm, which correspond to parameter perturbations lower than 10% in the symmetry of shape and injection velocities, the order of the mixing time was conserved with a mixing time variation of 14%. For greater deviations, the mixing time was dramatically increased from 64% up to 500%. Thus, we recommend normalized symmetry errors of less than 10% be achieved to ensure a mixing time close to the optimal value.

B. Flow injection velocities

We studied the influence of injection velocities on mixing time. The optimized injection velocities obtained in Ref. 4 were $u_s = 5.2$ m s^{-1} and $u_c = 0.2$ m s^{-1} (equivalent to a ratio $u_c/u_s = 0.0389$). For this, we considered the optimized mixer and varied its side injection velocity $u_s =$ from 0.5 m/s to 9.5 m/s, with a step size of 0.5 m/s. Then, we chose u_s in order to achieve u_c/u_s ratios in the set $\{25\%, 50\%, 75\%, 100\%, 250\%\}$ (considered as typical values) of the optimal ratio. This part of our study required a total of 95 evaluations of our model.

The results are summarized in Table III and Figure 10. We can see that for $u_s \in [4,9]$ m/s and $u_c \in [0.12, 0.88]$ m/s (i.e., a ratio u_c/u_s of [0.0292,0.0973]), the mixing time has exhibited variations lower than 10%. This suggests our mixer should be robust to small perturbations in the injection velocities. In particular, the velocity of the central inlet flow should be in the interval [0.1,0.8]m/s to obtain a reasonable mixing time. Moreover, from those results we can deduce that if the ratio and/or u_s are too small, the mixing time is drastically increased (more than 1000%). In fact, the mixer performance becomes similar to the one achieved in a previous study (see Ref. 8).

We conclude that accurate control of flow rates is crucial to achieving fast mixing. We recommend that flow rates be analyzed by experimental quantitation of inlet velocities using, for example, micron-resolution particle image velocimetry (as performed by Hertzog *et al.* in Ref. 6).

C. Thermophysical parameters

We next studied the stability of the mixing time of the optimized mixer to changes in the thermophysical coefficients of the denaturant solution or in the concentration values needed to control the folding process. In physical experiments, these changes may result from uncertainties in conditions or solution properties (temperature, pressure, dilution, etc.)[15] Subsections IV C 1 and IV C 2 summarize.

TABLE III. Variation in percent of the mixing time value (relative to the value of the optimal mixer indicated by ...) as a function of values of the side injection velocity u_s (m/s) and the injection ratio u_c/u_s.

	Ratio				
u_c (m/s)	0.0097	0.0195	0.0292	0.0389	0.0973
0.5	26 317	5444.8	1542.7	668.7	126.6
1	6 136.1	1518.6	278.4	134.2	40.5
1.5	2 776.7	667.4	109	56.8	20.8
2	1 631.1	388.7	57.4	30.5	12.4
2.5	1 083.7	229.5	34.6	18	7.8
3	775.2	142.6	22.2	11.1	4.9
3.5	583.3	91.1	14.8	6.6	3
4	456.8	59.7	9.8	3.6	1.5
4.5	368.9	41.6	6.2	1.8	0.4
5	304.6	30	3.6	...	0.5
5.5	256.6	22	1.6	1.4	1.3
6	219.5	16.4	1	2.4	1.9
6.5	190.4	12.2	1.1	3.2	2.4
7	166.8	9	2.1	3.9	2.9
7.5	147.5	6.4	2.9	4.5	3.3
8	131.6	4.4	3.6	5	3.6
8.5	118.1	2.8	4.2	5.4	3.9
9	106.7	5	4.7	5.7	4.2
9.5	97	9.2	9.4	10	42

1. Denaturant solution parameters

We chose for our work guanidine hydrochloride (GdCl) as a typical denaturant[1,12] described by the following parameters: diffusivity in background buffer of $D = 2 \times 10^{-9}\ \mathrm{m^2\,s^{-1}}$, denaturant solution dynamic viscosity of $\eta = 9.8 \times 10^{-4}\ \mathrm{kg\,m^{-1}\,s^{-1}}$, and mass density of $\rho = 1010\ \mathrm{kg\,m^{-3}}$.

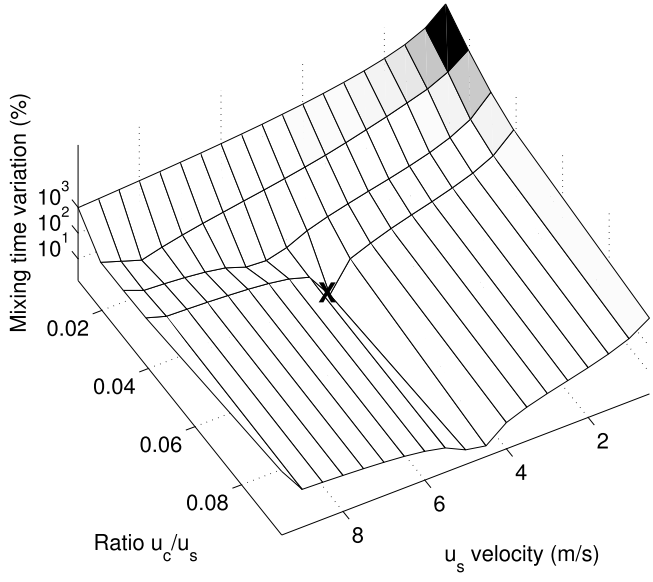

FIG. 10. Percent variation of the mixing time relative to the optimal mixer (represented by X) as a function of variations of the side injection velocity u_s (m/s) and the injection ratio u_c/u_s. Precise control of flow rates is crucial in mixing experiments.

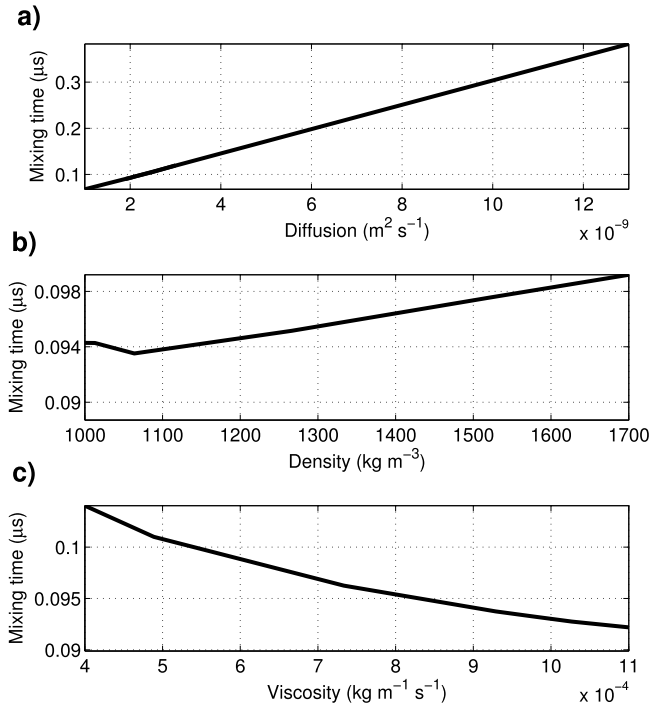

FIG. 11. Mean mixing time (in s) obtained as a function of denaturant solution (a) diffusivity, (b) mass density, and (c) dynamic viscosity and fixing the other two parameters.

The thermophysical properties of GdCl solutions vary with concentration and ambient temperature: consistent with the experimental work of Refs. 12, 16, and 17, (i) the density of the GdCl solutions can vary within [1000,1700] kg m^{-3}; (ii) its viscosity can vary in $[4, 11] \times 10^{-4}$ kg m^{-1} s^{-1}; and (iii) its diffusivity can vary in $[1.9, 13] \times 10^{-9}$ m^2 s^{-1}.

We considered the impact of these parameter variations on mixing time. We varied each parameter within the aforementioned intervals using seven equispaced values. All possible configurations of parameters values were studied, which represents a total of 343 evaluations of the model. Then, similar to the work presented in Section IV A 3, we computed the mean evolution of mixing time for each parameter value format both its lower and upper bounds and while varying the remaining coefficients to all their possible values.

The variations of the mean mixing time of the diffusion, density, and viscosity are presented in Figure 11. We see that the diffusion was the most sensitive parameter and can increase mixing time by up to 0.3 μs. The other two coefficients maintained the mean mixing time close to 0.1 μs. We note all of these values reasonable for the design as the order of mixing time is preserved. We further note increasing viscosity and decreasing diffusivity and density result in lower mixing time. The effect of decreasing diffusivity may at first seem counterintuitive but mixing time is the result of a geometry- and flow-rate-dependent convective diffusion process. For example, high diffusivity can result in significant decreases of denaturant concentration within the early focusing region of the center jet, where fluid velocities are still too low to stretch material interfaces and decrease diffusion lengths of the center jet. The latter effect is discussed by Hertzog *et al.*[5] (e.g., see Figure 2 of that reference).

2. Concentration threshold

Finally, we characterize the sensitivity of the mixer to the maximum and minimum denaturant concentration values of our mixing time (see (4)). The original mixer was designed to trigger unfolding for a concentration reduction of 60%. We here consider mixing times for denaturant concentration reductions ranging from 10% and 92%. To this end, for a particular threshold value denoted by γ, we

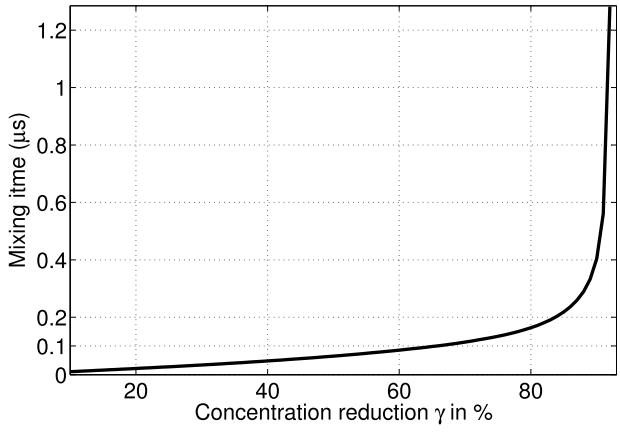

FIG. 12. Mixing time (in s) as a function of the percentage reduction in concentration as defined in Section IV C 2. The concentration values inherent to the definition of mixing have significant effect on mixing time. Note the maximum concentration reduction allowed by complete mixing far downstream is 92%.

identify α_γ and ω_γ such that $\alpha_\gamma - \omega_\gamma = \gamma$ and they produce the minimum mixing time value

$$J_\gamma(\phi) = \int_{c^\phi_{\omega_\gamma}}^{c^\phi_{\alpha_\gamma}} \frac{\mathrm{d}y}{\mathbf{u}^\phi(y)}, \tag{7}$$

where $c^\phi_{\alpha_\gamma}$ and $c^\phi_{\omega_\gamma}$ denote the Y-coordinates of the points situated along the streamline defined by the intersection of the two symmetry planes $z = 0$ μm and $x = 0$ μm, i.e., the y-axis, where the denaturant normalized concentration is α_γ and ω_γ, respectively.

Results are presented in Figure 12. The mixer exhibited mixing times lower than 0.4 μs for up to a reduction of 90%. We conclude that it is a robust design as the maximum reduction allowed by the flow rate ratios in this mixer was 92%. For a 70% denaturant concentration reduction, we observed a 0.1 μs mixing time. The latter can be compared to the mixer of Ref. 4 which showed mixing times of 1 μs for the same denaturant concentration reduction.[7]

V. CONCLUSIONS

We presented a detailed sensitivity study quantifying the robustness and performance of a microfluidic mixer design first presented in Ref. 4. In particular, we studied (i) the uniformity of the mixing time through the center inlet flow and (ii) the sensitivity of the mixing time with respect to key mixer parameters. The uniformity study showed that mixing time is quite stable throughout the majority of the inlet stream (up to a distance from the walls of 0.4 μm). With respect to design robustness, we found that the details of the mixer design in the region near the channel intersections are essential to the performance, i.e., the shape of the minimum channel widths near this inlet, the inlet flow velocity ratio, and possible (unwanted) asymmetries in the fabrication. Other factors such as inlet channel angles, mixer depth (above a certain minimum), fluid properties, and denaturant concentration thresholds for protein folding have significantly weaker effect on mixing time.

Our analyses may provide a guide to designers and fabricators of protein folding mixer devices and can be used to evaluate trade-offs between manufacturing quality, precision of flow control, and expected performance. Our work also serves as a case study associated with the general design and performance prediction of microfluidic devices and may serve as a guide to designing complex and optimal fluidic systems. In the least, the work highlights the complexity and importance of predicting and managing uncertainty in the performance of microfluidic systems.

In Table IV, for each parameter, we provide the mean, maximum, and standard deviation values of the mixing time percentage variation regarding the optimal mixer obtained with this sensitivity analysis.

TABLE IV. Summary of major findings of our sensitivity analysis: mean (Mean), standard deviation (Dev), and worst-case maximum (Max) values of the mixing time in percentage of base design. For the sake of completeness, we also report the optimal value of each parameter (Opt) as well as the range of the considered values (Range).

Parameter	Opt	Range	Mean	Dev	Max
		Intersection angle			
θ	$\pi/5$	[0,2π/5]	3	3	16
		Channel intersection			
Prot_{up}	0.8	[0,1]	21	17	51
Prot_{low}	0.7	[0,1]	30	26	79
		Channel width			
ω_c (μm)	2	[1,4]	50	67	150
ω_s (μm)	3	[1,4]	53	57	181
ω_o (μm)	10	[2,18]	28	41	101
		Mixer depth			
Depth (μm)	10	[8,12]	13	13	34
		Symmetry			
Symmetry (%)	0	[0.5,50]	216	196	542
		Injection velocities			
u_c (m s^{-1})	0.2	[0.005,0.92]	68	133	304
u_s (m s^{-1})	5.2	[0.5,9.5]	51	153	669
		Physical coefficients			
D (m^2 s^{-1})	2×10^{-9}	$[1.9,13]\times10^{-9}$	155	198	307
ν (kg m^1 s^{-1})	9.8×10^{-4}	$[4,11]\times10^{-4}$	4	4	11
ρ (kg m^{-3})	1010	[1000,1700]	2	2	6
γ (%)	60	[10,92]	129	271	1282

ACKNOWLEDGMENTS

We gratefully acknowledge the financial support of the Spanish "Ministry of Science and Innovation" under Project Nos. MTM2011-22658 and TIN2012-37483; the "Junta de Andalucía" and "European Regional Development Fund (ERDF)" through Project Nos. P10-TIC-6002, P11-TIC-7176, and P12-TIC30, and the research group MOMAT (Reference No. 910480) supported by "Banco Santander" and "Universidad Complutense de Madrid." Juana L. Redondo is a fellow of the Spanish "Ramón y Cajal" contract program, co-financed by the European Social Fund.

[1] J. Dunbar, H. P. Yennawar, S. Banerjee, J. Luo, and G. K. Farber, "The effect of denaturants on protein structure," Protein Sci. **6**(8), 1727–1733 (1997).
[2] J. A. Infante, B. Ivorra, A. M. Ramos, and J. M. Rey, "On the modeling and simulation of high pressure processes and inactivation of enzymes in food engineering," Math. Models Methods Appl. Sci. **19**(12), 2203–2229 (2009).
[3] J. P. Brody, P. Yager, R. E. Goldstein, and R. H. Austin, "Biotechnology at low reynolds numbers," Biophys. J. **71**(6), 3430–3441 (1996).
[4] B. Ivorra, J. L. Redondo, J. G. Santiago, P. M. Ortigosa, and A. M. Ramos, "Two- and three-dimensional modeling and optimization applied to the design of a fast hydrodynamic focusing microfluidic mixer for protein folding," Phys. Fluids **25**(3), 1–17 (2013).
[5] D. E. Hertzog, B. Ivorra, B. Mohammadi, O. Bakajin, and J. G. Santiago, "Optimization of a microfluidic mixer for studying protein folding kinetics," Anal. Chem. **78**(13), 4299–4306 (2006).
[6] D. E. Hertzog, X. Michalet, M. Jäger, X. Kong, J. G. Santiago, S. Weiss, and O. Bakajin, "Femtomole mixer for microsecond kinetic studies of protein folding," Anal. Chem. **76**(24), 7169–7178 (2004).
[7] S. Yao and O. Bakajin, "Improvements in mixing time and mixing uniformity in devices designed for studies of proteins folding kinetics," Anal. Chem. **79**(1), 5753–5759 (2007).

[8] B. Ivorra, B. Mohammadi, J. G. Santiago, and D. E. Hertzog, "Semi-deterministic and genetic algorithms for global optimization of microfluidic protein folding devices," Int. J. Numer. Method Eng. **66**(2), 319–333 (2006).
[9] B. Ivorra, A. M. Ramos, and B. Mohammadi, "Semideterministic global optimization method: Application to a control problem of the burgers equation," J. Optim. Theory Appl. **135**(3), 549–561 (2007).
[10] B. Ivorra, B. Mohammadi, and A. M. Ramos, "Optimization strategies in credit portfolio management," J. Global Optim. **43**(2), 415–427 (2009).
[11] J. L. Redondo, J. Fernández, I. García, and P. M. Ortigosa, "A robust and efficient global optimization algorithm for planar competitive location problems," Ann. Oper. Res. **167**(1), 87–105 (2009).
[12] K. Kawahara and C. Tanford, "Viscosity and density of aqueous solutions of urea and guanidine hydrochloride," J. Biol. Chem. **241**(13), 3228–3232 (1966).
[13] B. Massey and J. Ward-Smith, *Mechanics of Fluids*, 8th ed. (Taylor & Francis, 2005).
[14] H. Y. Park, X. Qiu, E. Rhoades, J. Korlach, L. Kwok, W. R. Zipfel, W. W. Webb, and L. Pollack, "Achieving uniform mixing in a microfluidic device: Hydrodynamic focusing prior to mixing," Anal. Chem. **78**(13), 4465–4473 (2006).
[15] A. Rogacs and J. G. Santiago, "Temperature effects on electrophoresis," Anal. Chem. **85**(10), 5103–5113 (2013).
[16] S. Sato, C. J. Sayid, and D. P. Raleigh, "The failure of simple empirical relationships to predict the viscosity of mixed aqueous solutions of guanidine hydrochloride and glucose has important implications for the study of protein folding," Protein Sci. **43**(9), 1601–1603 (2000).
[17] G. Gannon, J. A. Larsson, J. C. Greer, and D. Thompson, "Guanidinium chloride molecular diffusion in aqueous and mixed water-ethanol solutions," J. Phys. Chem. B **112**(30), 8906–8911 (2008).